IOP Publishing Measurement Science and Technology

Meas. Sci. Technol. **26** (2015) 015302 (15pp) doi:10.1088/0957-0233/26/1/015302

Tracking errors in 2D multiple particle tracking microrheology

Anne Kowalczyk, Claude Oelschlaeger and Norbert Willenbacher

Karlsruhe Institute of Technology (KIT), Institute of Mechanical Process Engineering and Mechanics, Gotthard-Franz-Straße 3, 76128 Karlsruhe, Germany

E-mail: claude.oelschlaeger@kit.edu

Received 6 August 2014, revised 20 October 2014
Accepted for publication 4 November 2014
Published 1 December 2014

Abstract

Tracking errors due to particles moving in and out of the focal plane are a fundamental problem of multiple particle tracking microrheology. Here, we present a new approach to treat these errors so that a statistically significant number of particle trajectories with reasonable length are received, which is important for an unbiased analysis of multiple particle tracking data from inhomogeneous fluids. Starting from Crocker and Grier's tracking algorithm, we identify particle displacements between subsequent images as artificial jumps; if this displacement deviates more than four standard deviations from the mean value, trajectories are terminated at such positions. In a further processing step, trajectories separated by a time gap $\Delta\tau_{max}$ are merged based on an adaptive search radius criterion accounting for individual particle mobility. For a series of Newtonian fluids covering the viscosity range 6–1300 mPa s, this approach yields the correct viscosity but also results in a viscosity-independent number of trajectories equal to the average number of particles in an image with a minimum length covering at least two orders of magnitude in time. This allows for an unbiased characterization of heterogeneous fluids. For a Carbopol ETD 2050 solution we recover the expected broad variation of particle mobility. Consistent with the widely accepted structural model of highly swollen microgel particles suspended in a polymer solution, we find about 2/3 of the tracers are elastically trapped.

Keywords: multiple particle tracking (MPT), microrheology, tracking error, heterogeneous fluids

(Some figures may appear in colour only in the online journal)

1. Introduction

Many complex fluids are heterogeneous on a μm scale. This is especially true for biological systems such as protein filament networks and also for polymers from biological or synthetic resources, which are used, for example, as thickeners in food, in personal and health care, plant protection or coating and adhesive formulations. The size, shape and structure of these heterogeneities determine the bulk flow properties, the processing and the application behavior of such products and hence are the key to a rational design of these materials. Multiple particle tracking (MPT) video microscopy has been introduced as microrheological tool which allows for a characterization of such microstructural and micromechanical heterogeneities since it gives direct access to the trajectories and mean squared displacements (MSD) of embedded tracer particles subject to thermal motion. MPT was originally described by Mason *et al* [1], Apgar *et al* [2], Ma *et al* [3] and Valentine *et al* [4] and so far it has been mainly used to study biological matter, such as the microheterogeneity of actin filament networks [4–8], living cells [7, 9–11], proteins [12, 13], DNA solutions [14] and biological gels [15, 16], but also used for synthetic polymer systems like Carbopol [17–19]. Often Newtonian fluids have been used as reference in these studies. The fluid mechanics of microrheology and especially the principles and applications of particle tracking microrheology have been described thoroughly [20, 21].

The basic idea of MPT is to study—by means of digital video microscopy—the equilibrium thermal response of colloidal tracer particles embedded in a material and thereby obtain quantitative information about the rheological properties of the surrounding fluid. The foundations of this technique were introduced in the mid 1990s when Mason and Weitz proposed a quantitative relation between the tracer MSD $\langle \Delta r^2(\tau) \rangle$ as a function of lag time τ and the complex shear modulus $G^*(\omega)$ as a function of frequency ω for systems homogeneous on the length scale of the tracer particles [22]: The Laplace transform of the particle MSD $\langle \Delta \tilde{r}^2(\mathrm{i}\omega) \rangle$ is related to the complex modulus G^* of the sample via a generalized Stokes–Einstein equation (GSE):

$$G^*(\omega) = \frac{k_B T}{\pi a \mathrm{i}\omega \langle \Delta \tilde{r}^2(\mathrm{i}\omega) \rangle} = G'(\omega) + \mathrm{i}G''(\omega) \qquad (1)$$

with a the radius of the embedded beads and k_B as the Boltzmann constant and T as temperature. In the ideal limiting cases $\langle \Delta r^2(\tau) \rangle \sim \tau^{\alpha}$. In the following the exponent α is termed a diffusive parameter, for purely viscous fluid $\alpha = 1$ and $\alpha = 0$, if the particles are embedded in an elastic solid [23]. For viscoelastic fluids α is a function of τ.

Generally, for homogenous materials bulk shear moduli agree very well with the particle tracking determined G' and G'' [24, 25]. This is also true for various other microrheological techniques; in particular for diffusing wave spectroscopy (DWS) or fluorescence correlation spectroscopy (FCS), good agreement between linear viscoelastic moduli of homogenous materials obtained there with and bulk rheological data has been reported for homogeneous model systems [1, 22, 26–29]. However, significant deviations between results from MPT and bulk mechanical measurements are reported for a variety of fluids [15, 25]. This is not surprising for inhomogeneous fluids where the GSE fails, but statistical analysis of individual tracer trajectories still allows for a characterization of local rheological properties on 0.1–1 μm length scale [4, 17–19]. But various studies have also undoubtedly shown that inaccuracies in particle tracking can lead to errors that alter the physical interpretation of results significantly [30], even for homogenous fluids. So-called static and dynamic errors, caused by noise and the finite exposure time of the imaging setup, can considerably influence the apparent dynamics of tracer particles [31–33].

The static error—corresponding to the apparent random motion of particles due to the noise of the camera and digitization effects—determines the upper limit for the accessible modulus G'. Typical formulations of coatings, adhesives, cosmetic or pharmaceutical products exhibit elastic moduli up to several 100 Pa. Application of MPT in these technically important fields requires an accuracy of MSD determination in the range of $10^{-5}\,\mu\mathrm{m}^2$, which can only be obtained with careful correction of static errors [33]. The static error depends on the hardware equipment—especially the quality of the CCD-chip and pixel size, the electronic components of the imaging system, the particle size and fluorescence properties and drifts or mechanical vibrations of the microscopy setup and also on the algorithm used to determine the particle position. As a consequence of the static error, even immobilized particles which do not move at all appear to have a finite MSD. In general, the finite spatial resolution $\bar{\varepsilon}$ is determined by measuring the MSD of immobilized particles $\langle \Delta r^2(\tau_0) \rangle = 4\bar{\varepsilon}^2$ at the shortest lag time τ_0 in two dimensions. For moving particles, the static error $4\bar{\varepsilon}^2$ superimposes an additional apparent random motion on the particle trajectories, which causes a systematic error in the derived diffusion coefficients [31, 33–35]. This error is not only relevant for highly elastic fluids but also generally at short lag times τ where the tracer particle displacement is still small [21].

As the tracers move during the imaging process, the digital image shows an average of the tracers' position during the exposure time σ. The related uncertainty in particle tracking is called dynamic error. Savin and Doyle have shown both theoretically and experimentally that the apparent MSD of tracer particles in a Newtonian fluid at lag time $\tau > \sigma$ has to be written as [31, 32]:

$$\langle \Delta \hat{\tilde{r}}^2(\tau, \sigma) \rangle = 4D(\tau - \sigma/3) + 4\bar{\varepsilon}^2 \qquad (2)$$

where D is the self-diffusion coefficient calculated from Stokes–Einstein relation $D = k_B T/(6\pi a \eta)$, and η is the viscosity of the surrounding liquid. But from a practical point of view, it is sufficient to deal with lag times $\tau > \sigma$. For non-Newtonian fluids, the situation is even more subtle with a lack in experimental investigations. The apparent MSD then depends on a delicate balance between the relaxation time of the medium and the exposure time in the experimental setup. Recent Monte Carlo simulations for both Voigt- and Maxwell-type fluids have revealed that the apparent MSD may underestimate the dynamics by orders of magnitude in the case where σ is comparable to the elastic relaxation time λ_S of the medium [32]. Although the static error increases with decreasing σ, this is usually not a serious limitation since the static error is relevant for highly elastic fluids with long relaxation times and correspondingly σ can be set to a sufficiently high value, for which $\sigma << \lambda_S$ still holds. Therefore, the dynamic error will not be discussed further in this paper.

In addition to static and dynamic errors which are a result of the imaging process, there are tracking errors occurring from an inaccurate trajectory assessment. During MPT measurements, only a small 2D area of the sample is observed. Since the tracer particles exhibit a 3D motion, they may not stay in the plane of observation during the whole measurement but may leave it and go to the sample reservoir above or below the focal plane. On the other hand, particles from the reservoir may enter the plane of observation at any time. This may lead to artificial 'jumps' in the trajectories which result in an increasing apparent mobility of the particles corresponding to an under estimation of the viscoelastic moduli. These trajectory artefacts can also lead to misinterpretation of fluid properties: the apparent acceleration of tracer particles has been attributed to the release of elastic energy of the investigated protein filament network [36] but may just have been a tracking error. Basically, the construction of a particle trajectory requires a particle tracking algorithm that includes a criterion how to connect particle positions identified in

subsequent images. In general, only particle positions identified in subsequent images which are closer to each other than the average particle separation d_{av} are accepted for trajectory construction and d_{av} is calculated from the particle concentration assuming a uniform distribution of particles throughout the sample. Usually, a certain fraction f_d of this maximum separation is selected as a criterion for the tracking algorithm. The probability that particle positions in subsequent images which do not correspond to one and the same particle are falsely connected increases with increasing search radius $r_s = f_d d_{av}$. Then, long trajectories including large steps (so-called 'jumps') are obtained and the particle mobility is overestimated. These jumps are due to particles occasionally moving in or out the focal plane and the probability of their occurrence increases with decreasing fluid viscosity. If r_s is set so low that the effect of jumps on the determination of G^* can be neglected, correct values for G' and G'' are obtained from the MSD of the corresponding trajectories. But then these trajectories are terminated after a short sequence of images and accordingly the lower limit of the frequency range for which the moduli can be determined accurately increases. Whenever a particle position is detected in an image which cannot be connected to an existing trajectory, a new trajectory is started and as a consequence the number of resulting trajectories may exceed significantly the average number of particles in the field of view. While this is no serious restriction for homogenous fluids, it can lead to a severe misinterpretation of the MPT results for inhomogeneous fluids. For example, the number of particles within low viscosity regions can be overestimated compared to the fraction of particles which are embedded in a more viscous or even predominantly elastic environment. Hence the corresponding volume fractions of regions with different rheological properties are erroneously calculated.

A thorough systematic determination of trajectory artefacts and a robust strategy to handle them are mandatory to improve the reliability of 2D MPT results, especially for the characterization of inhomogeneous fluids. Inappropriate treatment of the tracking error can lead to a wrong determination of the number of fast particles in an environment of low viscosity and also for other tracers in a more elastic surrounding, which simulate a freely moving particle due to the apparent acceleration inferred from artificial jumps. Savin and Doyle have suggested a concept which allows for the calculation of a single inhomogeneity parameter based on 2D particle tracking data [37]. The so-called heterogeneity ratio [38] includes the average and the variance of the MSD distribution where each MSD is weighted by the length of the corresponding trajectory; this allows for a quantitative dimensionless measure of spatial heterogeneity (also shown in Rich *et al* [39]). But the determination of the true distribution of the MSDs in an inhomogeneous fluid and the assessment of a representative spatial distribution of particle mobility characterizing the size and the shape of sample inhomogeneities is still lacking. 3D particle tracking, such as video holographic microscopy, confocal microscopy or off-focus imaging seem to be promising methods, but they still require a great technical effort and also the same proof of reliability regarding error treatment [40–47].

Here, we present a new approach to treat tracking errors in MPT experiments so that a physically meaningful number of particle trajectories of reasonable length is recovered. Artificial 'jumps' are eliminated using a mobility-dependent reduced radius of interest. First, we demonstrate the reliability of our data treatment algorithm using a series of Newtonian liquids with viscosities between 6 and 1300 mPa s. Then we use it to characterize the microheterogeneity of an aqueous solution of the commercial acrylic thickener Carbopol ETD ($c = 0.5$ wt%, pH ≈ 6). This thickener solution shows predominantly elastic behavior in bulk rheology. Previous studies [17–19] have revealed that viscous regions co-exist with highly elastic areas in such solutions. Appropriate treatment of tracking errors is mandatory to determine reliably the number of tracers in the viscous regions and their mobility. This is necessary to estimate the total volume and the composition of these regions.

2. Experiment

2.1. Samples

The MPT operating principle and the treatment of tracking errors are first discussed using glycerol-water mixtures as purely viscous homogenous model fluids.

A highly elastic aqueous solution of a tri-block-copolymer, Pluoronics® F127 (BASF SE, Ludwigshafen, Germany) has been employed to determine the static error which in turn sets the upper limit for the storage modulus accessible with a given setup. Tracer particles embedded in this polymeric hydrogel are treated as immobilized in order to determine the static error. An aqueous solution of the polymer with a concentration of 25 wt.% was prepared and tracer particles were added at a temperature $T = 7\,°C$. At this temperature the polymer dissolves quickly and the mixture is in the sol state so the tracer particles are distributed fast and homogenously. The system undergoes a sol-gel transition around $T = 15\,°C$ and the frequency-independent storage modulus at the measuring temperature $T = 20\,°C$ is $G' \approx 10^4$ Pa.

An aqueous solution of the commercial acrylic thickener Carbopol ETD 2050 (Lubrizol Advanced Materials, Cleveland, Ohio) was used to demonstrate the relevance of appropriate error treatment for inhomogeneous fluids. This alkali-swellable thickener consists of homo- and co-polymers of acrylic acid and a small amount of a crosslinking agent [48]. Upon neutralization, the weak acrylic acid groups dissociate in the aqueous environment, the polymer chains become soluble and cross-linked microgel particles start to swell, which gives rise to the thickening properties. Carbopol ETD 2050 is supplied as powder. We prepared samples by slowly adding 0.5 wt.% of powder in water, which decreases the pH to 3 while stirring. The mixture was further stirred at room temperature for 48 h and adjusted to pH = 6 by slowly adding 4 N NaOH. The resulting highly elastic microgel system is optically transparent but known to exhibit an inhomogeneous structure on the micrometer scale [18, 19].

As a reference for visoelastic but homogenous fluids, we have investigated aqueous solutions of the acrylic thickener

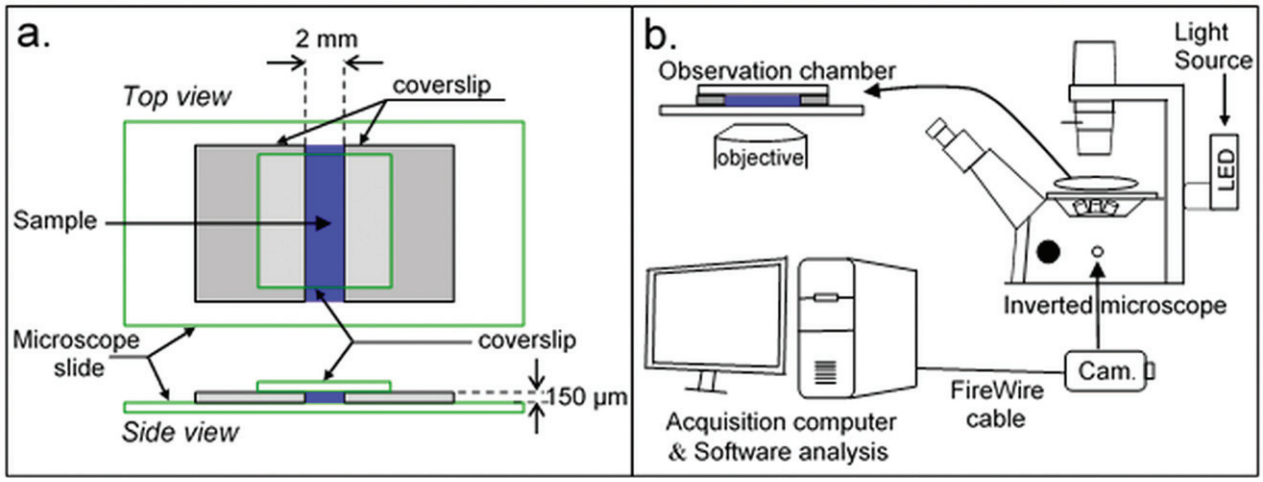

Figure 1. (*a*) Custom made microscope observation chamber for MPT experiments. The resulting chamber is approximately 2 mm wide and 150 μm high. (*b*) Schematic of the video microscopy setup for MPT. The sample is observed through a fluorescent inverted microscope equipped with a progressive scan camera. The camera is connected to a high performance computer via FireWire cable where movies are analyzed via custom tracking software.

Sterocoll D (BASF-SE). Sample preparation was done as described by Kheirandish *et al* [49] and polymer concentrations of 0.25%, 0.5% and 3% were chosen.

2.2. Mechanical rheology measurements

Steady and oscillatory shear measurements were performed at a temperature of 20 °C with a Haake MARS II rheometer (Thermo Electron) equipped with a cone-plate geometry (60 mm diameter, 1° cone angle).

2.3. Multiple particle tracking setup

In our study, we have used green fluorescent polystyrene microspheres of 0.19, 0.51 and 1.01 μm diameter (Bangs Laboratories: USA, lot Nr FC03F/7049) as tracer particles. The mixture (total volume: ~20 μl) containing the investigated fluid including the tracers (volume fraction around 1%) was injected into a self-build chamber (figure 1(*a*), consisting of a coverslip and microscope glass slide. The sample thickness was ~150 μm and the microscope was focused roughly halfway into the sample to minimize wall effects. Images of the fluorescent beads were recorded onto a personal computer via a progressive scan camera AVT Stingray F-033B (Allied Vision Technology: 1/2″ CCD, 656 × 492 square pixels, up to a frame rate of 84 f/s) mounted on an inverted fluorescence microscope (Axio Observer D1, Carl Zeiss), equipped with a Fluar 100×, NA 1.3, oil-immersion lens combined with a 1× optovar magnification changer. Our computer is equipped with a serial bus interface ATA (SATA-600, 600 MB s^{-1}, RAID 0) combined with three hard disk drives (HDD Toshiba 1TB SAS 6 GB s^{-1}) to allow for high-speed data acquisition and sufficient memory to store tracking sequences of 1000 frames in length. A detailed scheme of the MPT setup is shown in figure 1(*b*). For comparison, some MPT experiments were performed with a vaccum-cooled sCMOS camera (Andor: neo, full resolution of 2560 × 2160 square pixels, up to 50 f/s in global shutter mode). A LED light source (Colibri, Carl Zeiss) was used for illumination. This reduces the bleaching out of the fluorescence signal due to a pulsed illumination and low UV radiation intensity. This allows for longer measuring times corresponding to an extension of the accessible frequency range. Appropriate limiting upper and lower values for number and grey value of pixels have to be selected in order to distinguish individual tracer particles in the focal plane from aggregates and particles out of focus. Movies of the fluctuating microspheres were analyzed by a custom MPT routine incorporated into the software Image Processing System (Visiometrics iPS) which locates the center of mass of each particle in every picture. Particle tracing and calculation of MSD as well as the statistical analysis of the trajectories was done using a self-written Matlab® program based on the algorithm developed by Crocker and Grier [50] and converted to Matlab® by Blair (for further information: www.physics.emory.edu/~weeks/idl/index.html), designated in the following as Track algorithm (TR). Displacements of particle centers were monitored in a 60 × 45 μm field of view, for at least 1 min at a rate of 30 f/s. For each experiment, a total of about 100 particles were tracked simultaneously. Particle positions detected in subsequent images were connected to construct trajectories using a maximum distance criterion. If more than one particle was found within the selected search radius, the nearest particle position was used to continue the trajectory. Here, it should also be mentioned that the Track code has an integrated memory function allowing for connection of particles which temporarily disappear and reappear within the pre-defined maximum distance and thus are still considered as the same particle.

The static error, which depends on the previously introduced hardware equipment, was also determined in order to get the upper limit G_{max} of the accessible modulus. The static error $\langle \Delta r^2(\tau_0) \rangle$ for a given experimental setup can be determined from the MSD of immobilized particles. One can use either pinned particles or particles that are restricted in motion due

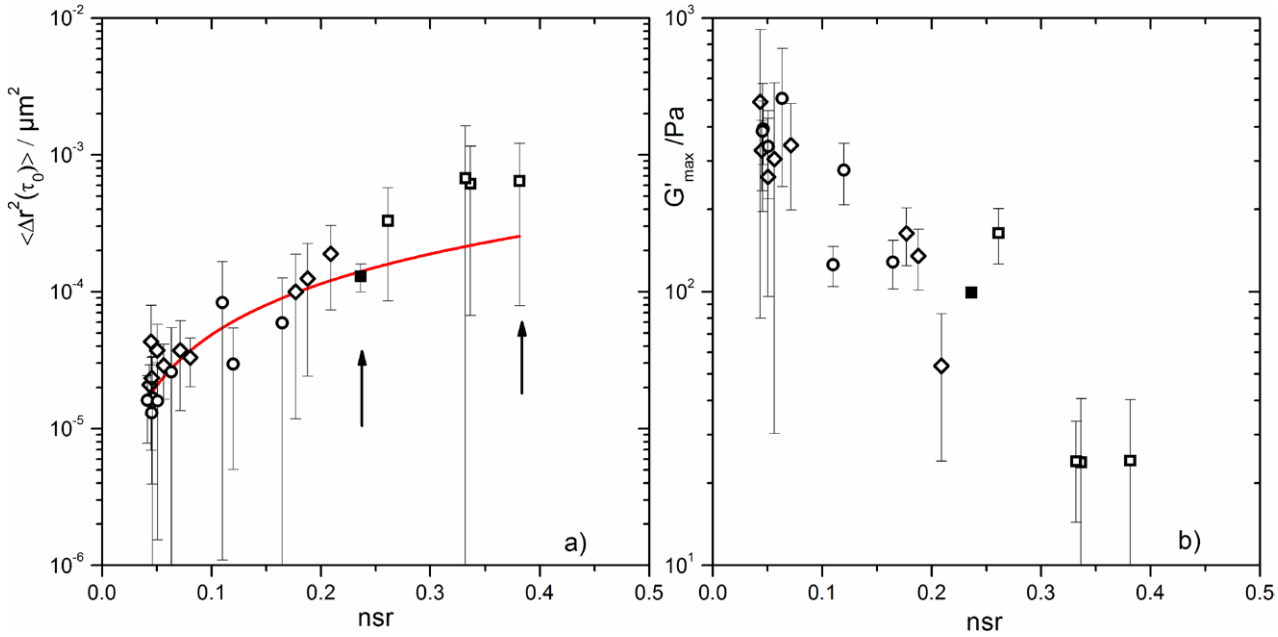

Figure 2. Static error $\langle \Delta r^2(\tau_0) \rangle$ (*a*) and maximum accessible modulus $G_{\max}$ (*b*) as a function of noise-to-signal ratio (nsr) for the following setup and acquisition parameters: Stingray progressive scan camera: 30 f/s, $\sigma \approx 33$ ms, gain = 0, particle sizes: 0.19 μm (open squares), 0.51 μm (open diamonds) and 1.01 μm (open circles) and Neo sCMOS camera: similar acquisition and particle size 0.19 μm (closed square).

to the surrounding fluid. In this latter case, imaging artefacts due to spherical aberration or distortion are avoided. Here, we have embedded the tracers into a polymer hydrogel which has a frequency independent modulus $G' \approx 10^4$ Pa at the measuring temperature 20 °C. The apparent motion of the embedded particles was recorded and the resulting MSD $\langle \Delta r^2(\tau_0) \rangle$ and the corresponding spatial resolution $\bar{\varepsilon} = \sqrt{\langle \Delta r^2(\tau_0) \rangle / 4}$ depend on the following acquisition parameters: shutter time, exposure time, frame rate, illuminating light intensity, gain of the output voltage as well as the fluorescence characteristics and size of tracer particles. All these parameters also influence the noise-to-signal power ratio (nsr). In figure 2(*a*) we show how the static error depends on nsr for different particle sizes. Here, nsr has been varied by variation of the light intensity; all other acquisition parameters were kept constant (frame rate: 30 f/s, exposure time: $\sigma \approx 33$ ms, gain = 0). The nsr has been calculated similarly as already described by Savin and Doyle [31]. A single image of the immobilized particles is analyzed and the variance of grey values of the background is compared to the signal from the embedded particles. We have used the Matlab® script provided by Gonzalez *et al* [51] to perform these calculations.

As expected, the static error increases with increasing nsr. For the setup used here, the noise-to-signal dependent static error $\langle \Delta r^2(\tau_0) \rangle$ is described by a power law relationship

$$\langle \Delta r^2(\tau_0) \rangle = 8.36 \times 10^{-4}\ \mu m^2\ nsr^{1.24}$$

which roughly holds for all particle sizes. But low nsr values are not accessible with small particles. The corresponding maximum accessible modulus $G_{\max}$ shown in figure 2(*b*) was calculated using the simplified general Stokes–Einstein equation assuming an ideal elastic solid [21]:

$$G_{\max} = \frac{2k_BT}{3\pi a \Delta r^2(\tau_0)} \tag{3}$$

The maximum accessible modulus increases with decreasing noise-to-signal ratio and is finally limited by the technical equipment. However, to reduce the noise-to-signal ratio for a given hardware setup, one can decrease the selected gain or the frame rate and increase the shutter time or lag times. Furthermore, it is advantageous to use larger particles for the characterization of highly elastic materials since the higher positioning accuracy prevails over the higher thermal mobility of smaller particles. Finally, it is recommended to select the setup and the acquisition parameters such that the maximum accessible modulus is at least one order of magnitude larger than the expected modulus of the fluid under investigation.

For comparison, we have determined the static error using the sCMOS camera Neo (Andor). Illuminating the sample with the same light intensity, the nsr is much lower compared to the CCD camera. This is clearly visible from the data points in figure 2(*a*) (marked by arrows). For a given nsr, the static error is independent of the camera, but the sCMOS camera provides much lower nsr for otherwise similar imaging conditions and the maximum accessible modulus is higher. The most important advantage of the sCMOS camera is its larger field of view (2560 × 2160 square pixels compared to 656 × 492 square pixels for the Stingray CCD camera) which allows for a simultaneous tracking of about 200 particles. Accordingly, the statistical significance of the extracted rheological quantities is improved and additionally rheological heterogeneities can be determined more accurately in the case of inhomogeneous fluids.

3. Results and discussion

3.1. Description and basics of the new tracking approach

The self-written code, called the radius of gyration (RG) criterion is a post process that allows for a high-quality tracking and a reliable quantitative characterization of inhomogeneous materials. The algorithm includes three steps based on the Track algorithm of Crocker and Grier (TR), but without using the integrated memory function:

1 Construction of particle trajectories based on a criterion of a maximum displacement. In this step, the average distance between tracer particles enters, but not the particle mobility.
2 Elimination of artificial 'jumps' identified by deviations from a Gaussian distribution of particle separations between subsequent images.
3 Joining adjacent short trajectories consecutively occurring in the stack of images within a preselected time gap. The distance criterion for joining trajectories is individually calculated for each trajectory based on its RG and only trajectories with similar mobility are connected.

In the first step of our particle tracking procedure, we consider a maximum displacement in a rheological unknown fluid, which we can estimate due to the particle density in the field of view. Every particle tracking algorithm includes a criterion how to connect particle positions identified in subsequent individual images. Assuming that the particles are uniformly distributed on a square grid, the average separation between the particles is $d_{av} = \sqrt{x \times y / n}$ (in μm or pixel) with x the length and y the width of the field of view and n the number of particles that are detected in the focal plane. A certain fraction f_d of this maximum separation is selected to define the so-called search radius $r_s = f_d d_{av}$. Particle positions in subsequent images with a separation less than r_s may be connected to one trajectory. Selecting a low r_s value reduces the number of artificial jumps, but on the other hand not all positions in subsequent images belonging to one particle may be connected, which can increase the number of trajectories artificially. Furthermore, if the particle is out of focus in one or more subsequent images, without the use of a memory setting the trajectory will be terminated and a new one will start as the particle reappears. Both tracking deficiencies result in trajectories substantially shorter than the total sequence of images, which corresponds to a loss of statistical information about the diffusion at long lag times. Therefore, further improvement of the tracking algorithm is necessary in order to determine not only the particle mobility but also the number of particle trajectories properly.

In figure 3, typical trajectories of probe particles in a purely viscous, homogenous glycerol-water mixture (7:3 with η_s = 22.5 ± 0.5 mPa s) are shown. Figures 3(*a*) and (*b*) display two different trajectories in the focal x-y-plane, which were determined using the Track algorithm with a maximum displacement of $r_s = 1.75\,\mu$m ($f_d = 0.3$). Dealing with the Brownian motion of tracer particles, we can assume a Gaussian distribution of particle displacements between subsequent images (i.e. trajectory steps) within a trajectory. Figures 3(*c*) and (*d*) show the corresponding particle displacement distributions observed between two subsequent images calculated from the respective particle positions. The trajectory shown in figure 3(*a*) includes two $d(\tau_0)$ values around 1 μm. The total number of trajectory steps is L = 1232. Assuming a Gaussian distribution of $d(\tau_0)$, results in a mean value $\tilde{d}(\tau_0) = 0.057\,34\,\mu$m and a standard deviation $d_\sigma(\tau_0) = 0.061\,47\,\mu$m. Accordingly, 99.994% of the detected displacement values $d(\tau_0)$ should be smaller than $\tilde{d}(\tau_0) + 4d_\sigma(\tau_0) = 0.3\,\mu$m. Even for a trajectory expanding over the full video sequence recorded with $L = L_{tot}$ = 2000 frames or steps, less than one event is expected with a displacement $d(\tau_0) > \tilde{d}(\tau_0) + 4d_\sigma(\tau_0)$. This clearly shows that this trajectory in figure 3(*a*) includes erroneous connections of particle positions obviously not corresponding to one and the same particle. But this is not the case for the trajectory shown in figure 3(*b*). In the following, all events with $d(\tau_0) > \tilde{d}(\tau_0) + 4d_\sigma(\tau_0)$ are treated as artificial jumps. Thereby, we locate and eliminate such jumps and cut the trajectory into shorter pieces. With shorter trajectories, long time information gets lost and the statistical significance of MSD data at high lag times τ is reduced. Moreover, the number of trajectories strongly increases and may exceed the average number of particles in the field of view by far.

Figures 3(*e*) and (*f*) present the MSDs and the corresponding viscosity values. As expected, for the Newtonian glycerol-water mixture both MSD curves adopt a power-law behavior $\langle \Delta r^2(\tau) \rangle \propto \tau^\alpha$ as a function of lag time with an exponent α close to 1. The MSD (figure 3(*e*)) for the trajectory with jumps is about a factor of 2 higher than the MSD for the trajectory without any defects. $|\eta^*|$ data determined from the MSD without artificial jumps agree very well with the $|\eta^*|$ determined from oscillatory shear measurements, whereas the trajectory including tracking errors results in a $|\eta^*|$ value which is about a factor of 2 too low. This clearly demonstrates that an appropriate treatment of tracking errors is mandatory for an accurate microrheological characterization even of Newtonian fluids. In figure 4 the fraction of trajectories including artificial jumps is plotted as a function of f_d for pure glycerol obtained using the TR algorithm with $\Delta\tau_{mem} = 0$. As expected N_{jumps}/N_{av} strongly increases with decreasing f_d.

These tracking errors affect the determination of the viscosity and the apparent viscosity decreases substantially below the true value as f_d increases. Data sets corresponding to different d_{av} have been analyzed. But obviously this parameter has no systematic effect on the fraction of trajectories including jumps.

The effect of tracking error treatment and the rheological significance was analyzed for a series of Newtonian glycerol-water mixtures. The Track algorithm without memory function was used as described above for construction of the trajectories. Here $r_s = 0.3 \cdot d_{av}$ was used as the search radius, but similar results were obtained for $r_s = 0.1 \cdot d_{av}$ and $0.5 \cdot d_{av}$. The number and average length of the resulting trajectories after the use of the Track algorithm and elimination of jumps are listed in table 1. In order to reduce the numerical effort and

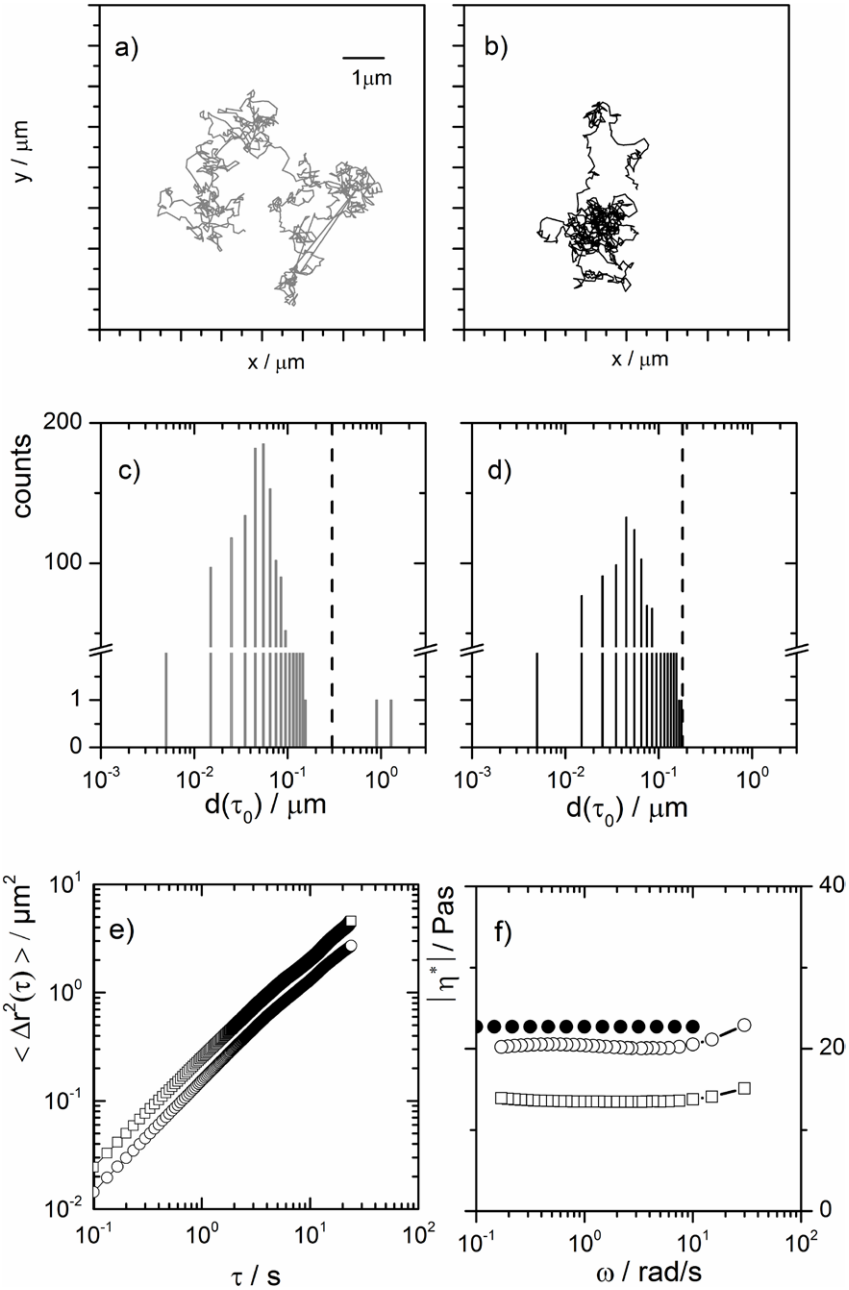

Figure 3. Typical trajectories of a 0.51 μm microsphere embedded in glycerol-water (7:3) mixture. (*a*) with jumps, (*b*) without jumps, (*c*) distribution of particle displacements and threshold $\tilde{d}(\tau_0) + 4d_\sigma(\tau_0)$ (dashed lines) with jumps, (*d*) without jumps, (*e*) lag time dependent MSD calculated from the particle trajectory with (open squares) and without (open circles) jumps, (*f*) corresponding absolute value of the complex viscosity in comparison to the data obtained from mechanical small amplitude oscillatory shear (closed circles).

to suppress statistical artefacts, we only include trajectories longer than $L_{\min} = 0.01\ L_{\text{tot}} = 20$ images.

The number of all identified trajectories N_{TR} using the Track algorithm normalized to the average number of particles N_{av} per image decreases and the average length $L_{\text{av,TR}}$ of trajectories increases with increasing fluid viscosity as expected. But even for the pure glycerol, the number of trajectories exceeds the average number of particles per image by more than a factor of five and the average length of the trajectories is only 12% of the total number of recorded images.

As shown in figure 4, these trajectories still include artificial jumps. Accordingly, the number of trajectories N_{c} after elimination of these jumps is higher than N_{TR} and the corrected average length $L_{\text{av,c}}$ is lower than $L_{\text{av,TR}}$. The fraction of artificial jumps in the trajectories constructed according to the Track algorithm and the relative change in trajectory length increases with increasing fluid viscosity. At this point it has to be noted that not all detected particle positions in individual images are included in a trajectory. The fraction of particle positions identified as part of a trajectory and hence the number of artificial jumps increases with increasing fluid

Table 1. Normalized number and average length of particle trajectories for different glycerol-water mixtures. N_{TR} and $L_{av,TR}$ refer to the results of the first tracking step using the maximum displacement criterion $r_s = 0.3 \cdot d_{av}$ according to the Track algorithm. N_c and $L_{av,c}$ designate the results after removal of artificial jumps as described in the text. N_{av} is the average number of particle positions detected in a single image and $L_{tot} = 2000$ frames, the length of the recorded image sequence. N_{RG} and $L_{av,RG}$ are the number and average length obtained using RG criterion with $\Delta\tau_{max} = 15$ and $L_{min} = 20$.

Glycerol-water mixture						
η_S / mPa s	N_{TR}/N_{av}	N_c/N_{TR}	N_{RG}/N_{TR}	$L_{av,TR}/L_{tot}$	$L_{av,c}/L_{av,TR}$	$L_{av,RG}/L_{av,TR}$
5.47 ± 0.46	19.17	1.03	0.81	0.041	0.98	1.52
10.3 ± 0.63	13.85	1.05	0.73	0.055	0.95	1.41
22.7 ± 1.33	13.25	1.03	0.83	0.058	0.97	1.44
59.5 ± 3.17	9.44	1.06	0.85	0.074	0.94	1.39
200.1 ± 14.67	6.17	1.15	0.88	0.121	0.87	1.27
1304 ± 71.02	5.85	1.22	0.81	0.124	0.82	1.34

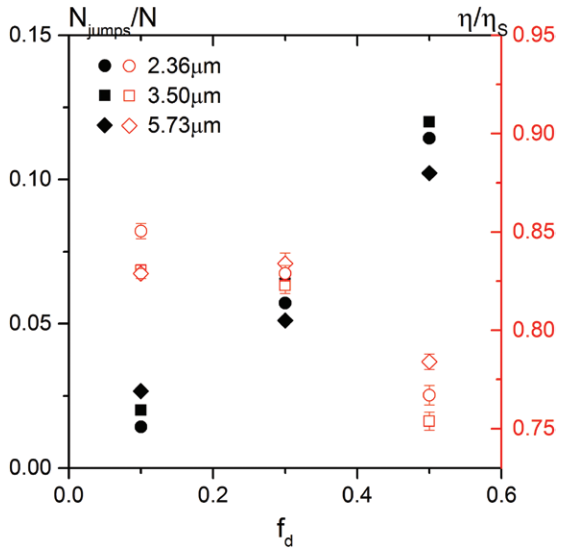

Figure 4. Pure glycerol solution MPT data obtained from TR algorithm with $\Delta\tau_{mem} = 0$ and $L_{min} = 0.01\ L_{tot}$: normalized number of trajectories without jumps (left y-axes, black) and the normalized viscosity (right y-axes, red) as a function of the fraction f_d for three different d_{av}.

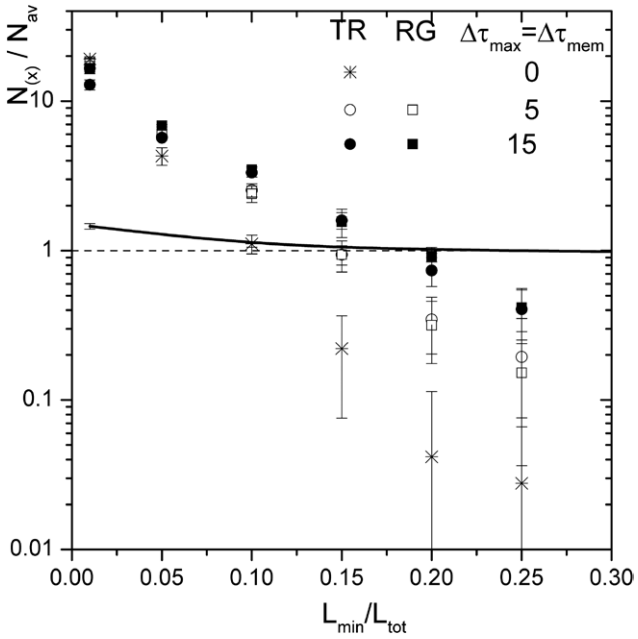

Figure 5. Glycerol–water mixture (1:1): reduced number of particle trajectories N_x/N_{av} as function of the normalized length L_{min}/L_{tot} obtained for different $\Delta\tau_{max} = \Delta\tau_{mem}$. Track algorithm without integrated memory time (stars), with $\Delta\tau_{max} = \Delta\tau_{mem} = 5$ images (open symbols) and 15 images (closed symbols). TR data (circles) in comparison to data obtained using the RG criterion (squares). Elastic homogenous acrylic thickener solution (Sterocoll D, 3 wt.%): reduced number of particle trajectories N_x/N_{av} as a function of the normalized length L_{min}/L_{tot} obtained for $\Delta\tau_{max} = 15$ (solid line).

viscosity. This will be discussed in more detail below. The elimination of the artificial jumps leads to biased results for the number and length of particle trajectories. Therefore, we have developed a criterion to connect trajectories in a physical meaningful way in order to improve the statistical significance of the further trajectory analysis.

3.1.1. Radius of gyration criterion. The radius of gyration criterion is looking for a new rheologically reasonable tracing distance in a third processing step after regular tracking and removal of artificial jumps. We suggest this criterion in order to connect trajectories closely related in time and space which explore a similar rheological environment.

First the radius of gyration R_g is calculated for each trajectory i:

$$R_{g,i} = \left(\frac{1}{L_i} \sum_{k=1}^{L_i} |\vec{r_k} - \vec{r_c}|^2 \right)^{1/2}$$

where L_i is the length of trajectory i, $\vec{r_k}$ is the position of the particle i in step k of the trajectory and $\vec{r_c}$ is the center of mass of the trajectory. Then we define a reduced radius of gyration

$$r_{g,i} = \frac{R_{g,i}}{\sqrt{L_i}}$$

which characterizes the particle mobility per time step. The quantity $\sqrt{L_i}$ is chosen for normalization since $R_{g,i} \sim \sqrt{L_i}$ assuming free diffusion in a purely viscous fluid. Starting with the longest trajectory, we search for other trajectories within the maximum displacement r_s around the end

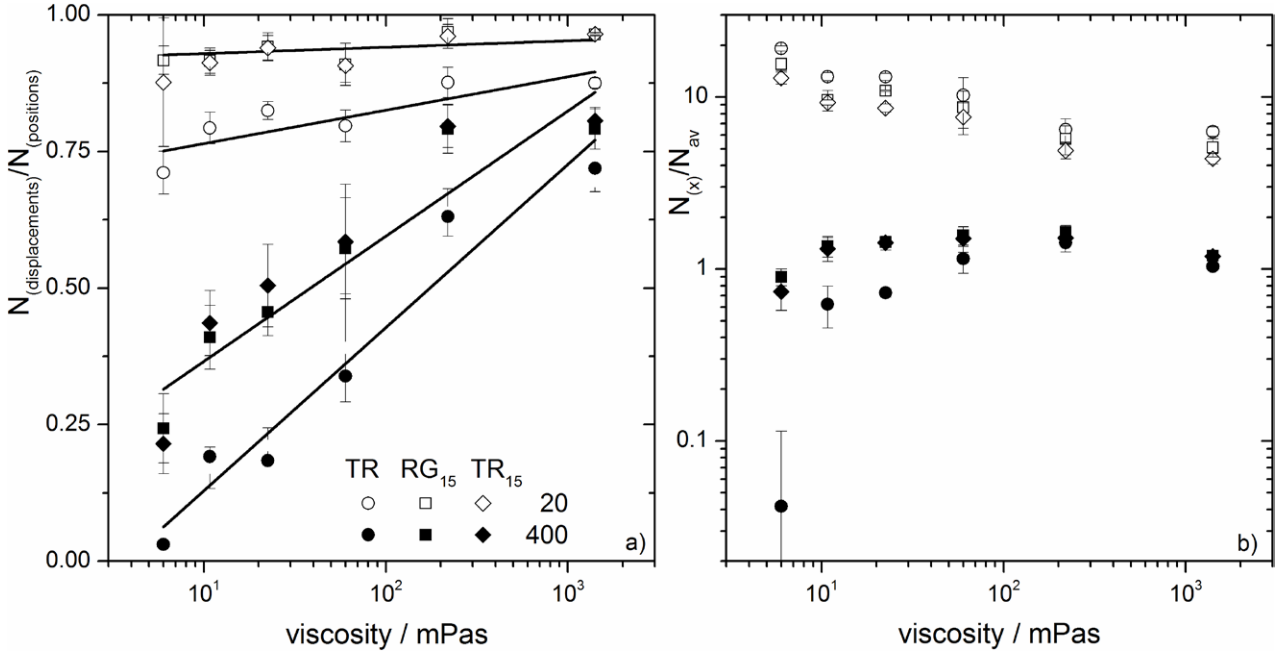

Figure 6. Glycerol water mixtures with different viscosity (*a*) fraction $N_{(\text{displacement})}/N_{(\text{positions})}$, (*b*) normalized number of particle trajectories obtained from Track (TR) algorithm with $\Delta\tau_{\text{mem}} = 0$ (circles), $\Delta\tau_{\text{mem}} = 15$ (diamonds) and from RG criterion with $\Delta\tau_{\text{max}} = 15$ (squares) with a minimum length of $L_{\text{min}} = 20$ (open symbols) or $L_{\text{min}} = 400$ (closed symbols).

points of trajectory i, which start within a time gap $\Delta\tau_{\text{max}}$ after trajectory i was terminated or end at a time $\Delta\tau_{\text{max}}$ before it was started. If another trajectory j is found in the vicinity of i with a time lag $\Delta\tau_{ij} \leq \Delta\tau_{\text{max}}$ we define search radii $r_{s,ij} = r_{g,i}\sqrt{\Delta\tau_{ij}}$ and $r_{s,ji} = r_{g,j}\sqrt{\Delta\tau_{ij}}$ around the end point of trajectory i and the starting point of trajectory j or vice versa. If these search areas overlap and if the reduced radii of gyration $r_{g,i}$ and $r_{g,j}$ agree within a certain range of confidence, these trajectories are connected. This second criterion is introduced in order to avoid merging of trajectories which are located close to each other, but obviously in different environments (e.g. at the phase boundary in an emulsion). If more than one trajectory j is found for which search radii $r_{s,ji}$ overlap within $\Delta\tau_{\text{max}}$ referring to the endpoints of trajectory i, the criteria described above are applied to all these trajectories. If the merging criteria are fulfilled for more than one of these trajectories, the trajectory j with the closest center of mass is selected to be connected to trajectory i. This procedure is different from the memory function included in the Track algorithm. This memory function allows for connection of particle positions within a predefined search radius not only in the subsequent image, but also if theses particle positions are found within r_s some time later. The time gap which is considered can be defined by the user and is called memory time $\Delta\tau_{\text{mem}}$. Typically $\Delta\tau_{\text{mem}} = 5$ images but does not account for the mobility of individual particles.

In the next sections, an appropriate choice of $\Delta\tau_{\text{max}}$ and L_{min} will be discussed to get a reasonable number of trajectories $N_x \approx N_{\text{av}}$ (x stands for RG, TR). This additional criterion is introduced with respect to the analysis of inhomogenous fluids. Below, it will be shown that $N_x \approx N_{\text{av}}$ for predominantly elastic fluids is irrespective of the selected tracking parameters.

3.2. Homogenous materials

For Newtonian fluids, the number of observed trajectories strongly decreases with increasing minimum length L_{min}. This is demonstrated for the glycerol-water mixture (1:1) with $\eta_0 = 5.47 \pm 1.7$ mPa s in figure 5. In contrast, $N_x/N_{\text{av}} \approx 1$ irrespective of L_{min} for a predominately elastic fluid, like the 3% Sterocoll D solution investigated here (solid line, figure 5). This immediately shows that particle tracking parameters have to be selected carefully in order to get unbiased results for inhomogeneous fluids with viscous and elastic regions. The reduced number of trajectories obtained with different tracking strategies is plotted versus L_{min}. N_x/N_{av} varies between 0.1 and 10 for this fluid and $L_{\text{min}} = 400$ (= 0.2 L_{tot}) has to be chosen in order to obtain a number of trajectories corresponding to N_{av}. The choice of L_{min} has a strong effect on the fraction of detected particle positions which is included in accepted trajectories. This is demonstrated in figure 6(*a*) where this fraction $N_{(\text{displacement})}/N_{(\text{positions})}$ is plotted as a function of viscosity for different tracking strategies. If $L_{\text{min}} = 0.01$ $L_{\text{tot}} = 20$, about 90% of the detected particle positions are included in trajectories irrespective of the sample viscosity. But especially at low viscosities, many short trajectories are created and accordingly their number exceeds the average number of particles per image by far. The quantity N_x/N_{av} decreases monotonically with increasing viscosity but with $L_{\text{min}} = 20$ it is always much larger than one figure 6(*b*).

This also shows up in the number and average length of the trajectories observed for the investigated glycerol-water mixtures summarized in table 1 for $\Delta\tau_{\text{max}} = 15$ and $L_{\text{min}} = 0.01$

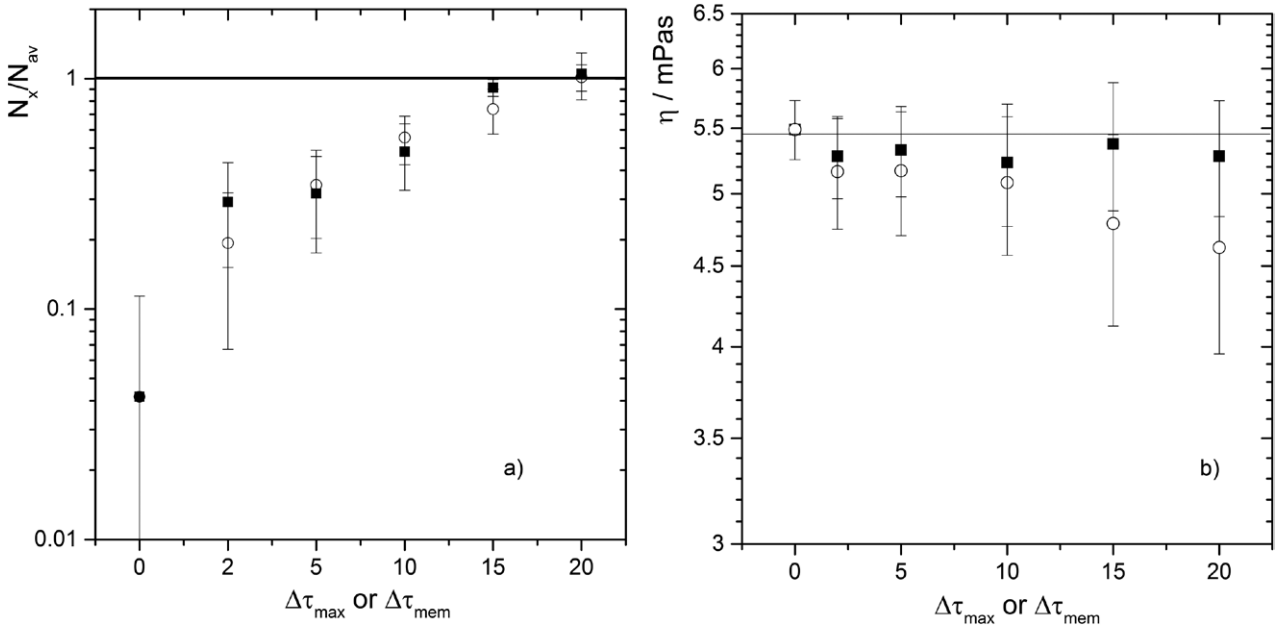

Figure 7. Glycerol–water mixture (1:1): (*a*) reduced number of particle trajectories obtained from RG or TR algorithm as function of $\Delta\tau_{max}$ (squares) or $\Delta\tau_{mem}$ (circles) with $L_{min} = 400$, (*b*) corresponding viscosity values obtained using the RG (squares) or Track algorithm (circles).

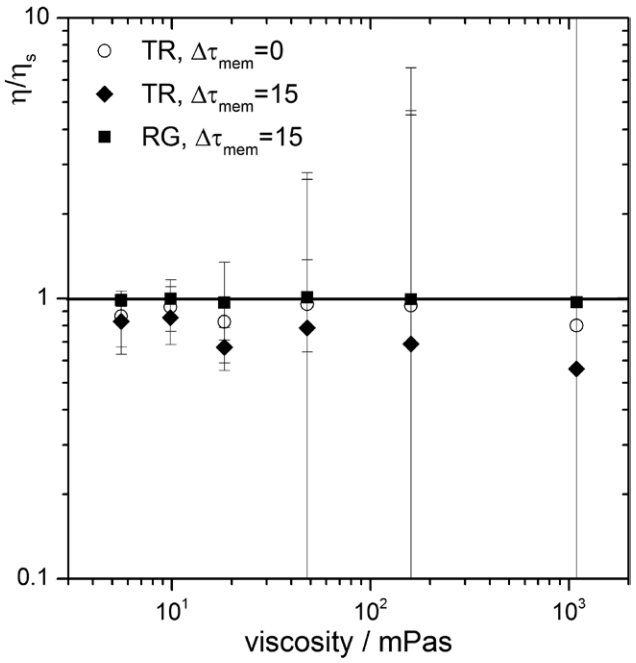

Figure 8. Normalized viscosity obtained from MPT as function of bulk shear viscosity of the investigated glycerol water mixtures: data from TR algorithm with (closed diamonds) and without (open circles) memory time, in comparison to results obtained using the RG criterion (squares).

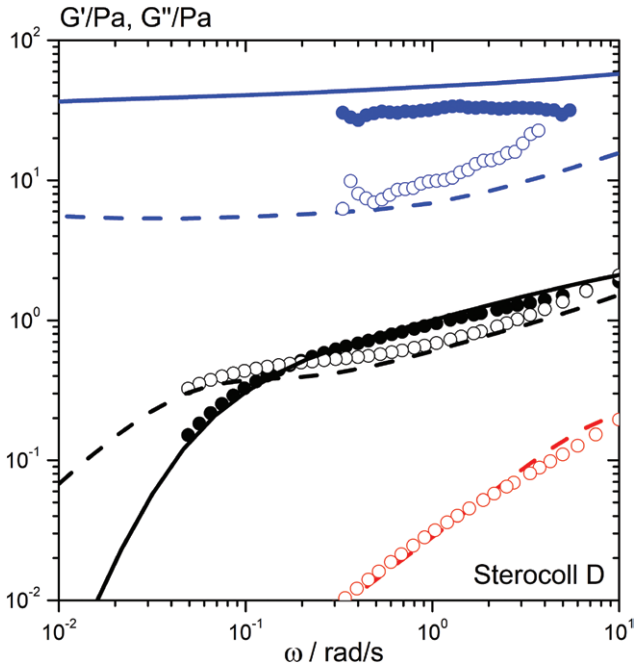

Figure 9. Storage G' and loss G'' (dashed line) modulus as a function of frequency for a homogenous acrylic thickener solution, Sterocoll D at three different concentrations 0.25% (red), 0.5% (black) and 3% (blue): mechanical determined G' (solid line) and G'' (dashed line), G' (closed circles) and G'' (open circles) data obtained from the applied RG criterion.

L_{tot}. The average length of trajectories increases by 30–50% when the RG criterion is applied to the trajectories obtained just using the standard Track algorithm. This number is reduced in all cases due to the application of the RG criterion but is always much larger than the average number of particles visible in a single image.

However, $N_{(displacements)}/N_{(positions)}$ decreases drastically, particularly for low viscosity fluids, when $L_{min} = 0.2\ L_{tot} = 400$ is selected. Then, the fraction of particle positions included in trajectories drops down to about 25% at low viscosities and to about 75% at the highest viscosities investigated. But the number of accepted trajectories corresponds to the average number of particles observed per image irrespective of the sample viscosity when either the RG criterion is applied or the memory function is used in the Track procedure.

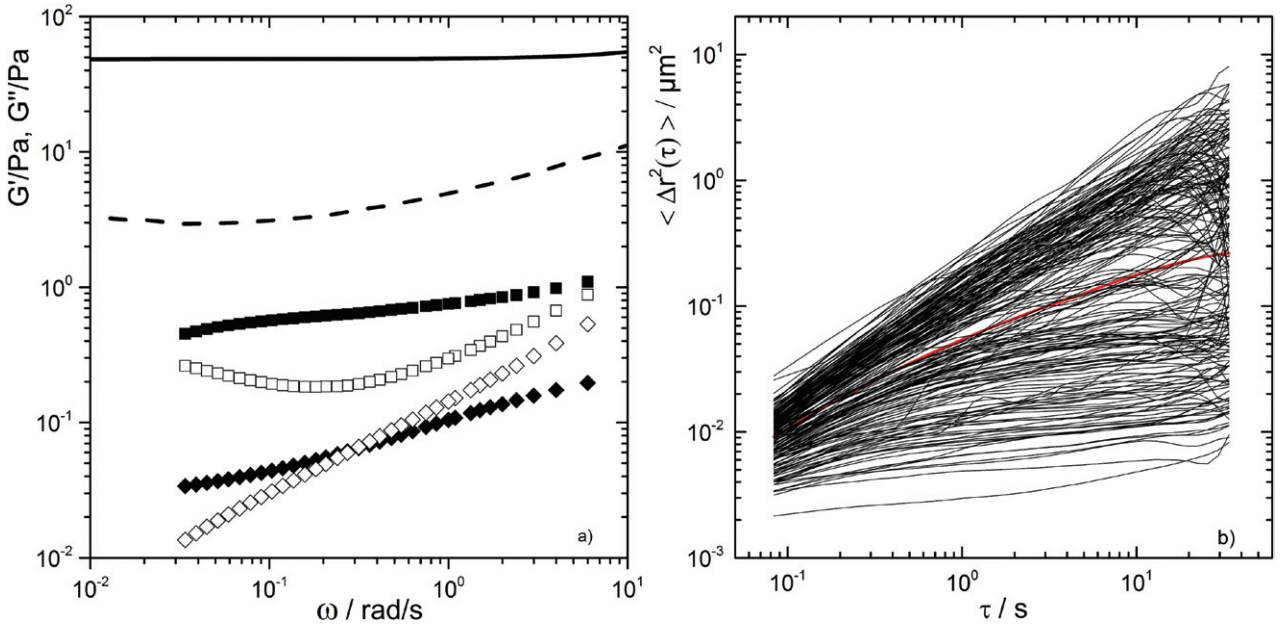

Figure 10. Carbopol ETD 2050, 0.5% in water at pH = 6: (*a*) frequency dependent G' (closed symbols) and G'' (open symbols) obtained from small amplitude oscillatory shear (lines), from the average MSD obtained in MPT measurements (diamonds) and from the average MSD of the elastic population identified in MPT experiments (squares); (*b*) lag time dependent MSDs.

Besides L_{min}, the time gap $\Delta\tau_{max}$ in the RG criterion or the memory time $\Delta\tau_{mem}$ in the standard tracing have a strong impact on the number of resulting trajectories. In both cases N_x/N_{av} increases strongly with an increasing time gap as demonstrated in figure 7(*a*) for the glycerol-water (1:1) mixture. Here L_{min} was set to $L_{min} = 0.2\ L_{tot} = 400$ and then $N_x/N_{av} \approx 1$ for $\Delta\tau_{max} = \Delta\tau_{mem} \geq 15$.

The disadvantage of the Track algorithm with the memory function is that increasing $\Delta\tau_{mem}$ leads to an increasing number of artificial jumps and as a consequence the resulting viscosity decreases with increasing $\Delta\tau_{mem}$. In contrast, the choice of $\Delta\tau_{max}$ has essentially no effect on η when the RG criterion is applied. For the glycerol-water (1:1) mixture, this is clearly demonstrated in figure 7(*b*) where the apparent viscosity is plotted versus $\Delta\tau_{max}$ or $\Delta\tau_{mem}$ respectively. Similar results have been obtained for the other glycerol-water mixtures investigated here. Analyzing the MPT experiments for this series of Newtonian fluids covering more than two decades in viscosity always leads to a good agreement with bulk viscosity data either if the RG criterion is used and $\Delta\tau_{max} = 15$ and $L_{min} = 0.2$ L_{tot} are selected as tracking parameters or the Track algorithm without the use of integrated memory time. The Track algorithm results in systematically lower viscosities and deviations from the true bulk viscosity increases with increasing viscosity using the memory function. These results clearly show up in figure 8 where the viscosity from MPT experiments normalized to the bulk viscosity is plotted versus the viscosity obtained from mechanical measurements for these different glycerol-water mixtures. The lower apparent viscosities obtained with the Track algorithm is due to the artificial jumps in trajectories. The fraction of such jumps increases with increasing fluid viscosity since the overall length of trajectories increases and thus the probability of artificial jumps increases.

In conclusion, we can state that the RG algorithm allows for an accurate determination of the viscosity of homogenous Newtonian fluids over a wide viscosity range using one and the same set of tracking parameters ($L_{min} = 0.2\ L_{tot}$, $\Delta\tau_{max} = 15$). A similarly good agreement with mechanical bulk viscosity data can be achieved with the Track algorithm setting $\Delta\tau_{mem} = 0$.

But in contrast to the Track algorithm, the RG algorithm with the tracking parameters selected above yields a constant number of trajectories consistent with the average number of particles observed in a single image in the whole investigated viscosity range. Finally, the mobility criterion mentioned above avoids the false connection of trajectories belonging to significantly different micro-environments. These latter two features of the RG algorithm are especially important when inhomogeneous fluids with locally varying rheological properties are investigated. The robustness of the RG algorithm demonstrated for Newtonian fluids suggests that it is also advantageous for avoiding biased results when trajectories of tracer particles with different mobility in inhomogeneous fluids are statistically analyzed.

Next, we compare results from our MPT experiments with bulk mechanical rheometry data for a series of homogenous acrylic thickener solutions varying from Newtonian to predominately elastic response with increasing polymer concentration. Corresponding results are shown in figure 9. These data demonstrate good agreement between G^* data from MPT and mechanical rheometry for a Newtonian, a weakly viscoelatic and a predominantly elastic fluid using the new algorithm presented above.

3.3. MPT in inhomogeneous fluids

In a homogenous fluid, either the static or the tracking error is dominant and can be accounted for by appropriate choice

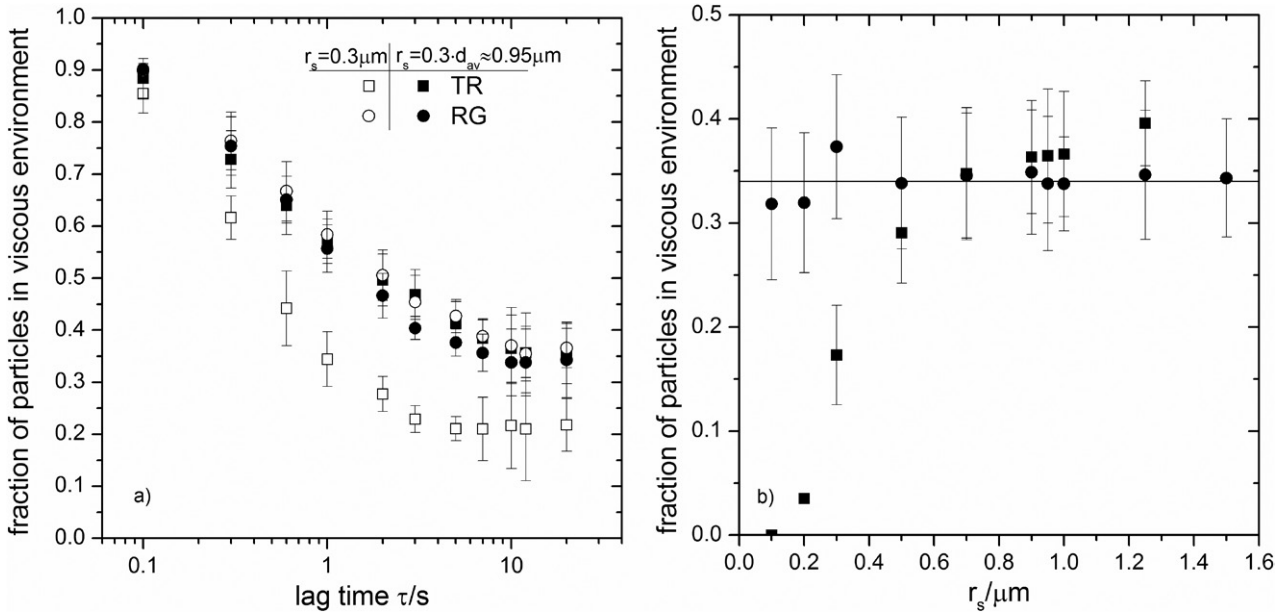

Figure 11. (*a*) Fraction of particles in a viscous environment as a function of lag time τ for two different search radii $r_s = 0.3\,\mu$m (open symbols) and $r_s = 0.3\ d_{av} = 0.95\,\mu$m (closed symbols). Results obtained with the RG algorithm (circles) and the Track algorithm (squares) setting $L_{min} = 400$ and $\Delta\tau_{max} = \Delta\tau_{mem} = 15$. (*b*) Fraction of particles in a viscous environment determined at $\tau = 10$ s with tracking parameters $\Delta\tau_{max} = \Delta\tau_{mem} = 15$, $L_{min} = 400$ as function of search radius r_s.

of the experimental setup, acquisition parameters or tracking algorithms. Here, we focus on the effect of errors in heterogeneous fluids and use an aqueous solution of the commercial acrylic thickener Carbopol ETD 2050 as a model system. This system has been subject to numerous micro- and macrorheological studies [17–19, 52–55]. These thickener solutions are well known as yield stress fluids with a gel-like behavior on a macroscopic scale. Additionally, previous studies have shown that these solutions are heterogeneous on the micrometer length scale. Oppong and Bruyn (2011) [17] investigated a concentration series (0.01–1wt.%) of Carbopol ETD 2050 using a probe size of 1 μm and analysed their data based on the Crocker and Grier algorithm. Roughly 50 tracer particles were monitored at a rate of ten frames per second for about 10 s (considered τ-range $0.2 < \tau < 5$ s). They found two populations of tracer particles with substantially different mobility in these solutions. The 'slow' fraction, which exhibits nearly lag time-independent MSDs, increases strongly at concentrations above 0.1 wt.% and the ratio of 'fast' to 'slow' determined at a lag time of $\tau = 1$ s is roughly 25:75 for a Carbopol concentration of 0.5 wt.% (pH =6) [17].

Here, we investigate a solution with a polymer concentration of 0.5 wt.% at pH ≈ 6 using macro- and microrheology. In figure 10(*a*) the frequency dependent storage G' and loss modulus G'' is shown. As expected, this fluid is highly elastic on the macroscopic scale, with G' independent of frequency and $G' > G''$. No crossover of G' and G'' is observed in the investigated frequency range. MPT experiments have been performed on this solution using 0.19 μm polystyrene particles. Particle trajectories were constructed using the Track algorithm in combination with the RG criterion. The corresponding MSD results shown in figure 10(*b*) were obtained using the parameters $r_S = 0.95\,\mu$m, $L_{min} = 0.2\ L_{tot} = 400$

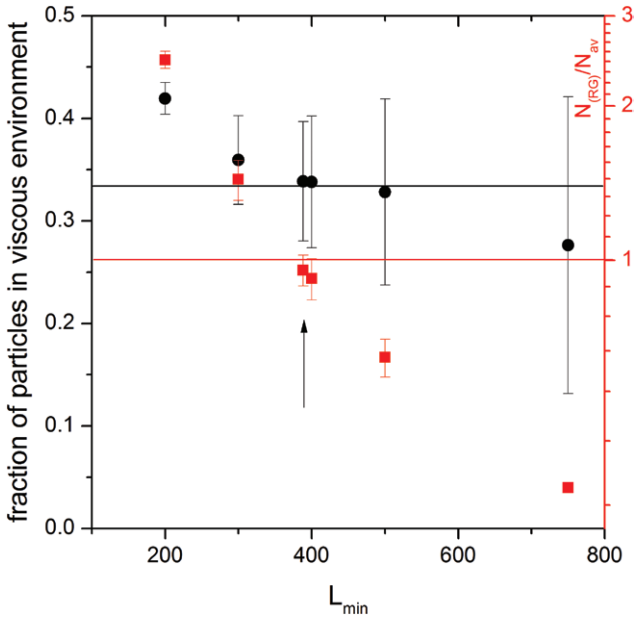

Figure 12. Fraction of particles in viscous environment (black circles, left *y*-axes) and the normalized number N_{RG}/N_{av} (red squares, right *y*-axes) as function of L_{min} obtained from MPT data using the RG criterion determined at $\tau = 10$ s with $\Delta\tau_{max} = 15$. $N_{RG} = N_{av}$ criterion is marked by an arrow.

($L_{tot} = 2000$, rate of 12 f/s) and $\Delta\tau_{max} = 15$. As expected, a broad variety of different MSDs is found in this solution. The initial MSD values vary about an order of magnitude, but the lowest values are still at least one order of magnitude higher than the resolution of our setup. Thus, the static error correction described previously can be neglected here.

According to the time evolution of the MSDs, the particles can be roughly divided into two classes or populations. For the

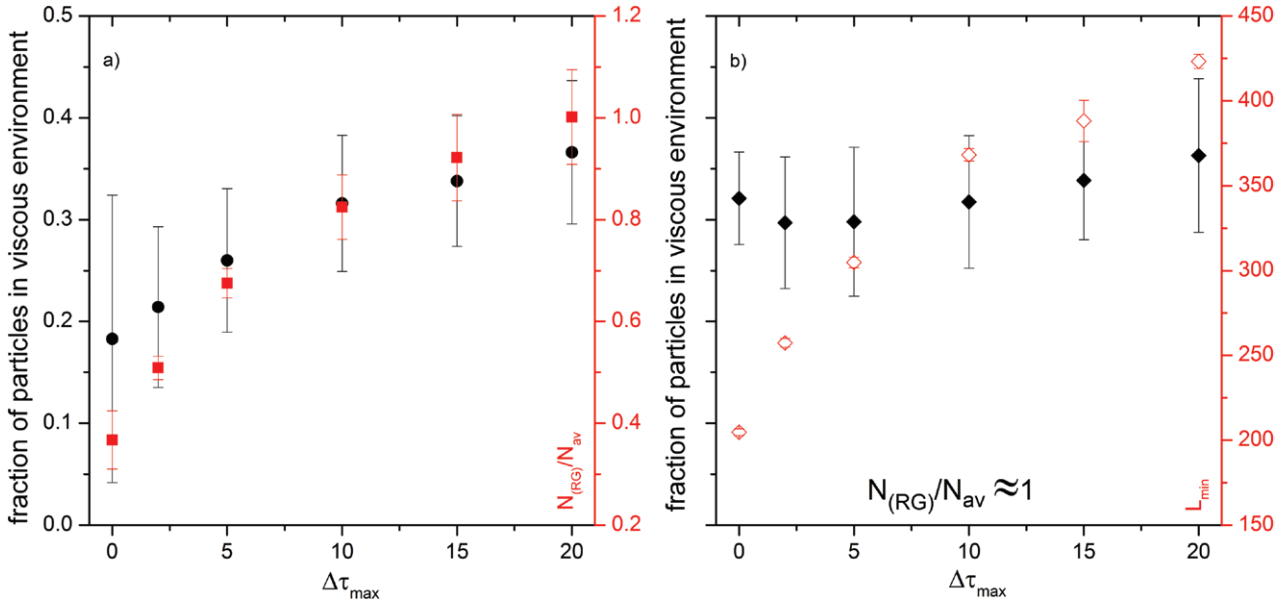

Figure 13. (*a*) Fraction of particles in viscous environment (black circles) and the normalized number of particles N_{RG}/N_{av} (red squares, right *y*-axes) with $L_{min} = 0.2$ $L_{tot} = 400$ as a function of $\Delta\tau_{max}$ determined at $\tau = 10$ s using RG criterion and (*b*) fraction of particles in viscous environment (black diamonds) and L_{min} (red diamonds, right *y*-axes) with $N_{RG} = N_{av}$ criterion as function of $\Delta\tau_{max}$ determined at $\tau = 10$ s using RG criterion.

first class $\langle \Delta r^2(\tau) \rangle \propto \tau^{\alpha}$ throughout the investigated τ-range $0.08 < \tau < 30$ s and α is close to one. These particles move in a viscous or weakly viscoelastic environment. For the second population, the MSDs tend toward a lag time-independent value, which means that these particles are exposed to a predominately elastic surrounding medium.

For the sake of completeness, the complex shear modulus calculated from the average MSD (red line in figure 10(*b*)) is included in figure 10(*a*). Obviously, the G' and G'' values are orders of magnitude lower and exhibit a completely different frequency dependence as compared to the mechanically determined bulk moduli. Similar results have already been reported by Oppong *et al* [19] and it is clear that such a simplified analysis is pointless for inhomogeneous fluids. Even the modulus data calculated from the average MSD of the elastic population (black squares in figure 10(*b*)) are almost two orders of magnitude below the bulk values. Obviously, the bulk viscoelastic response strongly depends on the detailed structure of the viscous and elastic regions.

In the following, we will discuss how the tracking parameters affect the distribution of particles among populations. For that, we divide the broad distribution in two populations with exponent $\alpha < 0.5$ and $\alpha > 0.5$ at a certain lag time. The lag time has a most prominent effect on the characterization of the populations. This is shown in figure 11(*a*). At $\tau = 0.1$ s almost 90% of the particles would be classified as 'fast-moving' in a viscous environment. But at a lag time of 1 s, only 50% of the particles exhibit a slope $\alpha > 0.5$. At these short times particles can diffusive freely, but finally they sense that they are elastically trapped and at lag times $\tau > 5$ s the fraction of 'fast' particles reaches a constant level of about 35%, similar to what has been reported earlier [17]. But note, if the Track algorithm is used with a too small search radius, the 'fast' fraction is underestimated. This is demonstrated in more detail in figure 11(*b*) corresponding to a lag time $\tau = 10$ s. The RG algorithm reveals a fraction of 35% of particles moving in a viscous environment, essentially independent of the selected search radius r_s. But when the Track algorithm is used, this fraction strongly increases with r_s and levels off at 35% only for $r_s > 0.5\,\mu$m ($f_d > 0.2$). Obviously, the Track algorithm leads to an underestimation of the 'fast' moving particles if the search radius is set too small. In contrast, the RG criterion reveals a fraction of 'fast' particles moving in a viscous environment independent of the search radius and that clearly simplifies the characterization of rheologically unknown fluids. For comparison, we have selected $\Delta\tau_{mem} = 15$ when analyzing the data using the TR algorithm. Usually $\Delta\tau_{mem} < 5$ is selected for such an analysis, but this would yield similar results with respect to the fraction of particles in a viscous environment for the thickener solutions investigated here. How results are affected by the choice of $\Delta\tau_{max}$ will be discussed in the subsequent section.

Furthermore, the result obtained at lag times $\tau > 5$ s is consistent with the generally accepted structural model: the neutralized Carbopol 'solutions' consist of highly swollen, crosslinked microgel particles suspended in a solution of non-crosslinked fractions of the polymer [19, 56, 57]. For the sample investigated here, about 2/3 of the tracers are located within the microparticles, whereas about 1/3 diffuses within the interfacial regions between the microgel particles. This roughly corresponds to a random close packing of monodispersed mircogel particles.

The robustness of the new tracking algorithm with respect to an adequate characterization of inhomogeneous fluids is further demonstrated considering the effect of the parameters L_{min} and $\Delta\tau_{max}$ on the classification of particle mobility. As shown in figure 12, the fraction of particles classified as being in a viscous environment weakly decreases with increasing L_{min}. At the same time, the ratio N_{RG}/N_{av} decreases and as

expected, the experimental error drastically increases since the number of long trajectories is low. This data set shows that the $L_{min} = 0.2\ L_{tot} = 400$ is a reasonable choice: the fraction of 'fast' particles can be determined with a relative uncertainty of about 10% and additionally the $N_{RG} = N_{av}$ criterion is fulfilled. The effect of the tracking parameter $\Delta\tau_{max}$ on the characterization of microheterogeneities at a fixed value $L_{min} = 0.2\ L_{tot}$ is shown in figure 13(*a*). The fraction of particles in a viscous environment increases with increasing $\Delta\tau_{max}$ and reaches a value of about 1/3 for $\Delta\tau_{max} > 10$ and for $\Delta\tau_{max} \geq 15$ also the $N_{RG} \approx N_{av}$ criterion is fulfilled. Finally, figure 13(*b*) demonstrates that the fraction of 'fast' particles moving in a viscous environment is essentially constant if the pair of tracking parameters $\Delta\tau_{max}$ and L_{min} is chosen such that the $N_{RG} = N_{av}$ criterion is always fulfilled. The minimum trajectory length has to be increased from $L_{min} = 200$ to $L_{min} = 420$ when $\Delta\tau_{max}$ is varied between 0 and 20 in order to meet this condition.

In conclusion, the tracking algorithm introduced here is robust and the selected tracking parameters $L_{min} = 0.2\ L_{tot}$ and $\Delta\tau_{max} = 15$ yield consistent results for a broad range of Newtonian fluids and the inhomogenous thickener solution investigated here. But it has to be kept in mind that these parameters have to be carefully adjusted if another hardware setup (microscope, camera) or other tracer particles are used.

4. Conclusions

Tracking errors due to particles moving in and out of the focal plane are a fundamental problem of MPT microrheology. Here, we have presented a new approach to treat these errors so that a statistically significant number of particle trajectories with reasonable length are received. Starting from the widely used Crocker and Grier tracking algorithm, we identify particle displacements between subsequent images as artificial jumps; if this displacement deviates more than four standard deviations from the mean value, trajectories are terminated at such positions. In a subsequent processing step, trajectories separated by a time gap $\Delta\tau_{max}$ are merged based on an adaptive search radius criterion taking into account a reduced radius of gyration of each trajectory and the individual particle mobility. Data analysis relies on a reasonable choice of $\Delta\tau_{max}$ and the accessible timescale depends on a minimum number of time steps or length L_{min} of the trajectories accepted for further analysis. For a series of Newtonian fluids covering the viscosity range from 6 to 1300 mPa s, this approach not only yields the correct viscosity but also results in a viscosity-independent number of trajectories N_{RG} with a minimum length such that MSD values in a time interval safely covering more than two orders of magnitude were received. For the experimental setup and the hardware used here, choosing $L_{min} = 400$ and $\Delta\tau_{max} = 15$ resulted in a number of particle trajectories matching the average number of particle positions detected in an individual image. This latter criterion is particularly independent. Generally, it is fulfilled if the particles are embedded in a predominantly elastic fluid, but not if the standard Crocker and Grier algorithm is used to track particles in a (low) viscosity environment. These features are crucial for an adequate unbiased characterization of inhomogeneous fluids. The new algorithm was applied to an aqueous solution of the commercial thickener Carbopol ETD 2050. Such solutions have been subject to extensive macro-and microrheological characterization and are known for their heterogeneity on a micrometer length scale. Accordingly, we found the expected broad variation of particle mobility. The MSD data are roughly divided in two classes or populations regarded as elastically trapped and freely diffusing. About 2/3 of the tracers are trapped. This is consistent with the widely accepted structural model of highly swollen, crosslinked microgel particles suspended in a solution of non-crosslinked polymer chains.

Acknowledgments

The authors would like to thank Lubrizol Advanced Materials for providing the Carbopol ETD 2050 sample and BASF for providing the Pluoronics and Sterocoll D sample. We acknowledge S Neser for the introduction to the Image Processing System software (Visiometrics iPS) and assistance with preliminary MPT experiments. S Volz provided technical assistance in programming the RG algorithm.

References

[1] Mason T G *et al* 1997b Particle tracking microrheology of complex fluids *Phys. Rev. Lett.* **79** 3282–85
[2] Apgar J *et al* 2000 Multiple-particle tracking measurements of heterogeneieties in solutions of actin filaments and actin bundles *Biophys. J.* **79** 1095–106
[3] Ma L *et al* 2001 A 'hot-spot' mutation alters the mechanical properties of keratin filament networks *Nat. Cell Biol.* **3** 503–6
[4] Valentine M *et al* 2001 Investigating the microenvironments of inhomogeneous soft materials with multiple particle tracking *Phys. Rev.* E **64** 061506
[5] Kole T P *et al* 2005 Intracellular mechanics of migrating fibroblasts *Mol. Biol. Cell* **16** 328–38
[6] Tseng Y and Wirtz D 2001 Mechanics and multiple-particle tracking microheterogeneity of alpha-actin-crosslinked actin filament networks *Biophys. J.* **81** 1643–56
[7] Tseng Y *et al* 2002b Local dynamics and viscoelastic properties of cell biological systems *Curr. Opin. Colloid Interface Sci.* **7** 210–7
[8] Tseng Y 2002a Microheterogeneity controls the rate of gelation of actin filament networks *J. Biol. Chem.* **277** 18143–50
[9] Heidemann S R and Wirtz D 2004 Towards a regional approach to cell mechanics *Trends Cell Biol.* **14** 160–6
[10] Tseng Y *et al* 2005 How actin crosslinking and bundling proteins cooperate to generate an enhanced cell mechanical response *Biochem. Biophys. Res. Commun.* **334** 183–92
[11] Lee J S H *et al* 2006 Ballistic intracellular nanorheology reveals ROCKhard cytoplasmic stiffening response to fluid flow *J. Cell Sci.* **119** 1761–8
[12] Xu J *et al* 2002 Microheterogeneity and microrheology of wheat gliadin suspensions studied by multiple-particle tracking *Biomacromolecules* **3** 92–9
[13] Dawson M, Wirtz D and Justin H 2003 Enhanced viscoelasticity of human cystic fibrotic sputum correlates with increasing microheterogeneity in particle transport *J. Biol. Chem.* **278** 50393–401

[14] Goodman A, Tseng Y and Wirtz D 2002 Effect of length, topology and concentration on the microviscosity and microheterogeneity of DNA solutions *J. Mol. Biol.* **323** 199–15
[15] Caggioni M *et al* 2007 Rheology and microrheology of a microstructured fluid: The gellan gum case *J. Rheol.* **51** 851–65
[16] Panorchan P, Wirtz D and Tseng Y 2004 Structure-function relationship of biological gels revealed by multiple-particle tracking and differential interference contrast microscopy: The case of human lamin networks *Phys. Rev.* E **70** 041906
[17] Oppong F K and Bruyn J R 2011 Mircorheology and jamming in a yield-stress fluid *Rheol. Acta* **50** 317–26
[18] Oppong F K and de Bruyn J R 2007 Diffusion of microscopic tracer particles in a yield-stress fluid *J. Non-Newton. Fluid Mech.* **142** 104–11
[19] Oppong F K *et al* 2006 Microrheology and structure of a yield-stress polymer gel *Phys. Rev.* E **73** 041405
[20] Squires T M and Mason T G 2010 Fluid mechanics of microrheology *Annu. Rev. Fluid Mech.* **42** 413–38
[21] Wirtz D 2009 Particle-tracking microrheology of living cells: principles and applications *Annu. Rev. Biophys.* **38** 301–26
[22] Mason T G and Weitz D 1995 Optical measurements of frequency-dependent linear viscoelastic moduli of complex fluids *Phys. Rev. Lett.* **74** 1250–53
[23] Mason T G 2000 Estimating viscoelastic moduli of complex fluids using the generalized Stokes–Einstein equation *Rheol. Acta* **39** 371–8
[24] Dasgupta B and Weitz D 2005 Microrheology of cross-linked polyacrylamide networks *Phys. Rev.* E **71** 021504
[25] Oelschlaeger C, Willenbacher N and Neser S 2008 Multiple-particle tracking (MPT) measurements of heterogeneities in acrylic thickener solutions *Progr. Colloid Polym. Sci.* **134** 74–9
[26] Mason T G, Gang H and Weitz D 1997a Diffusing-wave-spectroscopy measurements of viscoelasticity of complex fluids *J. Opt. Soc. Am.* A **14** 139–49
[27] Yamada S, Wirtz D and Kuo S C 2000 Mechanics of living cells measured by laser tracking microrheology *Biophys. J.* **78** 1736–47
[28] Oelschlaeger C *et al* 2009 Linear-to-branched micelles transition: a rheometry and diffusing wave spectroscopy (DWS) study *Langmuir* **25** 716–23
[29] Rathgeber S *et al* 2009 Microrheology with fluorescence correlation spectroscopy *Langmuir* **25** 6368–76
[30] Martin D G, Forstner M B and Käs J A 2002 Apparent subdiffusion inherent to single particle tracking *Biophys. J.* **83** 2109–17
[31] Savin T and Doyle P S 2005b Static and dynamic errors in particle tracking microrheology *Biophys. J.* **88** 623–38
[32] Savin T and Doyle P S 2005a Role of a finite exposure time on measuring an elastic modulus using microrheology *Phys. Rev.* E **71** 041106
[33] Wu P H *et al* 2009 A novel approach to high accuracy of video-based microrheology *Biophys. J.* **96** 5103–11
[34] Cheezum M K, Walker W F and Guilford W H 2001 Quantitative comparison of algorithms for tracking single fluorescent particles *Biophys. J.* **81** 2378–88
[35] Thompson R E, Larson D R and Webb W W 2002 precise nanometer localization analysis for individual fluorescent probes *Biophys. J.* **82** 2775–83
[36] Wong I *et al* 2004 Anomalous diffusion probes microstructure dynamics of entangled F-actin networks *Phys. Rev. Lett.* **92** 178101
[37] Savin T and Doyle P 2007 Statistical and sampling issues when using multiple particle tracking *Phys. Rev.* E **76** 021501
[38] Ehrenstein G W 1999 *Polymer-Werkstoffe: Struktur—Eigenschaften—Anwendungen* (München: Hanser)
[39] Rich J P, McKinley G H and Doyle P S 2011 Size dependence of microprobe dynamics during gelation of a discotic colloidal clay *J. Rheol.* **55** 273
[40] Cheong F C *et al* 2009 Flow visualization and flow cytometry with holographic video microscopy *Opt. Express* **17** 13071–9
[41] Lee S-H *et al* 2007 Characterizing and tracking single colloidal particles with video holographic microscopy *Opt. Express* **15** 18275–82
[42] Cheong F C, Krishnatreya B J and Grier D G 2010 Strategies for 3D particle tracking with holographic video microscopy *Opt. Express* **18** 13563–73
[43] Park J S and Kihm K D 2005 3D micro-PTV using deconvolution microscopy *Exp. Fluids* **40** 491–9
[44] Wu M, Roberts J W and Buckley M 2005 3D fluorescent particle tracking at micron-scale using a single camera *Exp. Fluids* **38** 461–5
[45] Gao Y and Kilfoil M L 2009 Accurate detection and complete tracking of large populations of features in 3D *Opt. Express* **17** 4685–704
[46] Dinsmore A D *et al* 2001 3D confocal microscopy of colloids *Appl. Opt.* **40** 4152–9
[47] Speidel M, Joná˘s A and Florin E-L 2003 3D tracking of fluorescent nanoparticles with subnanometer precision by use of off-focus imaging *Opt. Lett.* **28** 69–71
[48] Baudonnet L, Grossiord J-L and Rodriquez F 2004 Effect of dispersion stirring speed on the particle size distribution and rheological properties of three carbomers *J. Dispers. Sci. Technol.* **25** 183–92
[49] Kheirandish S, Gubaydullin I and Willenbacher N 2008 Shear and elongational flow behavior of acrylic thickener solutions Part II: effect of gel content *Rheol. Acta* **48** 397–407
[50] Crocker J C and Grier D G 1996 Methods of digital video microscopy for solloidal studies *J. Colloid Interface Sci.* **179** 298–10
[51] Gonzalez R C, Woods R E and Eddins S L 2009 *Digital Image Processing Using Matlab* 2nd edn (Knoxville, TN: Gatesmark)
[52] Roberts G P and Barnes M S 2001 New measurements of flow-curves for Carbopol dispersions without slip artefacts *Rheol. Acta* **40** 499–503
[53] Curran S J *et al* 2002 Properties of Carbopol solutions as models for yield-stress fluids *J. Food Sci.* **67** 176–80
[54] Gutowski I A *et al* 2012 Scaling and mesostructure of Carbopol dispersions *Rheol. Acta* **51** 441–50
[55] Kim J-Y *et al* 2003 Rheological properties and microstructures of Carbopol gel network system *Colloid Polym. Sci.* **281** 614–23
[56] Roberts G P and Barnes H A 2001 New measurements of flow-curves for Carbopol dispersions without slip artefacts *Rheol. Acta* **40** 499–503
[57] Carnali J O and Naser M S 1992 The use of dilute solution viscometry to characterize the network properties of Carbopol migrogels *Colloid Polym. Sci.* **270** 183–93